



**HAL**  
open science

## **Radiosensitizing Fe-Au nanocapsules (hybridosomes®) increase survival of GL261 brain tumor-bearing mice treated by radiotherapy**

Clément Goubault, Ulrich Jarry, Mégane Bostoën, Pierre-Antoine Éliat, Myrtil L Kahn, Rémy Pedeux, Thierry Guillaudeux, Fabienne Gauffre, Soizic Chevance

### ► To cite this version:

Clément Goubault, Ulrich Jarry, Mégane Bostoën, Pierre-Antoine Éliat, Myrtil L Kahn, et al.. Radiosensitizing Fe-Au nanocapsules (hybridosomes®) increase survival of GL261 brain tumor-bearing mice treated by radiotherapy. *Nanomedicine: Nanotechnology, Biology and Medicine*, 2022, 40, pp.102499. 10.1016/j.nano.2021.102499 . hal-03514563

**HAL Id: hal-03514563**

**<https://univ-rennes.hal.science/hal-03514563>**

Submitted on 25 Jan 2023

**HAL** is a multi-disciplinary open access archive for the deposit and dissemination of scientific research documents, whether they are published or not. The documents may come from teaching and research institutions in France or abroad, or from public or private research centers.

L'archive ouverte pluridisciplinaire **HAL**, est destinée au dépôt et à la diffusion de documents scientifiques de niveau recherche, publiés ou non, émanant des établissements d'enseignement et de recherche français ou étrangers, des laboratoires publics ou privés.

1 **Radiosensitizing Fe-Au Nanocapsules (Hybridosomes®) increase survival of GL261 brain**  
2 **tumor-bearing mice treated by radiotherapy**

3  
4 Clément Goubault<sup>1§</sup>, Ulrich Jarry<sup>2,3§</sup>, Mégane Bostoën<sup>2</sup>, Pierre-Antoine Éliat<sup>4</sup>, Myrtil L. Kahn<sup>5</sup>,  
5 Rémy Pedoux<sup>6</sup>, Thierry Guillaudeau<sup>2</sup>, Fabienne Gauffre<sup>1</sup> and Soizic Chevance<sup>1\*</sup>

6  
7 § Co-first author

8 <sup>1</sup>Univ Rennes, CNRS, ISCR-UMR6226, F-35000 Rennes, France.

9 <sup>2</sup>Univ Rennes, CNRS, INSERM, BIOSIT - UMS 3480, US\_S 018, Oncotrial, F-35000  
10 Rennes, France.

11 <sup>3</sup>Biotrial Pharmacology, Unité De Pharmacologie Préclinique, F-35000 Rennes, France.

12 <sup>4</sup>Univ Rennes, CNRS, INSERM, BIOSIT - UMS 3480, US\_S 018, Prism Bio-Scan, F-35000  
13 Rennes, France.

14 <sup>5</sup>LCC, CNRS, F-31000 Toulouse, France.

<sup>6</sup>Univ Rennes, INSERM, COSS – UMR\_S 1242, LCC Eugène Marquis, Rennes, France

15  
16 **Keywords:** Glioblastoma, Nanoparticles, Hybridosomes®, Combined therapies, Radiotherapy,  
17 Chemotherapy; Mouse Models, MRI and Bioluminescence

18 **Corresponding author:** Soizic Chevance                      soizic.chevance@univ-rennes1.fr

21 **Author contributions**

22 CG, UJ, PAE, MB and SC performed most experiments and analyses. MK synthesized the iron  
23 oxide nanoparticles. CG, UJ, TG, FG and SC designed and supervised the study. CG, UJ, PAE,  
24 FG and SC wrote and edited the manuscript.

25  
26 **Funding:** This work was supported by Biosit (Univ Rennes, CNRS, INSERM, BIOSIT - UMS  
27 3480, US\_S 018, F-35000 Rennes, France), the University of Rennes 1, the CNRS (Centre  
28 National de la Recherche Scientifique), the LCC (Laboratoire de Chimie de Coordination, UPR  
29 8241), and the Région Bretagne.

31 **Conflicts of Interest:** The authors disclose no potential conflicts of interest

32  
33 **Abbreviations:** BBB, Blood Brain Barrier; GBM, Glioblastoma; H®, Hybridosome®; H(Fe),  
34 Iron oxide Hybridosome®; H(Fe;Au), Iron Oxide and Gold Hybridosome®; IR; Irradiation;  
35 MRI, Magnetic Resonance Imaging; NP, nanoparticle(s); NTA, Nanoparticle Tracking  
36 Analysis; ROS, Reactive Oxygen Species; SPION, iron oxide superparamagnetic nanoparticles;  
37 TEM, Transmission Electron Microscopy.

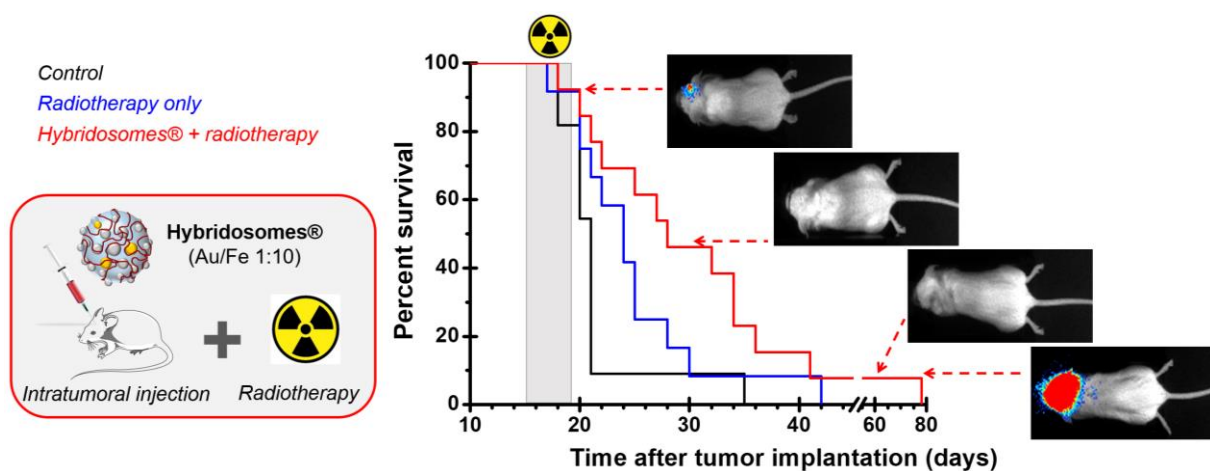
1

## 2 Acknowledgements

3 We warmly thank the staff of BIOSIT (Univ Rennes, CNRS, INSERM, BIOSIT - UMS 3480,  
4 US\_S 018, F-35000 Rennes, France): especially Stéphanie Dutertre and Xavier Pinson for  
5 confocal microscopy observations (MRic Photonic), Agnès Burel and Aurélien Dupont for  
6 transmission electron microscopy analysis (MRic TEM), Roselyne Viel and Alain Fautrel  
7 (H<sup>2</sup>P<sup>2</sup>) for tissue staining and imaging and all the staff of the Animal Facility of Rennes  
8 (ARCHE) for animal husbandry and care. We thank R. Hashizume (University of California,  
9 San Francisco, CA) for providing GL261-Luc<sup>+</sup> cells. We thank G. Casterou and O. Mongin for  
10 kindly providing the iron oxide NP, the PEG-PAA polymer and the BODIPY dye respectively.  
11 We are grateful to R. Pedeux (Univ Rennes, CNRS, INSERM, BIOSIT - UMS 3480, US\_S  
12 018, Oncotrial, F-35000 Rennes, France) and A. Le Goff (Biotrial Pharmacology, Biotrial,  
13 France) for supporting this project.

14

## 15 Graphical Abstract



16

17 **Legend:** Intratumoral injection of Iron Oxide – Gold nanocapsules (Hybridosomes®) with radiotherapy increase the survival  
18 of brain tumor-bearing mice. The bioluminescence can be monitored as the tumoral cells express luciferase.

19

## 20 Abstract

21 Glioblastoma remains a cancer for which the effectiveness of treatments has shown little  
22 improvement over the last decades. For this pathology, multiple therapies combining resection,  
23 chemotherapy and radiotherapy remain the norm. In this context, the use of high-Z  
24 nanoparticles such as gold or hafnium to potentiate radiotherapy is attracting more and more  
25 attention. Here, we evaluate the potentiating effect of hollow shells made of gold and iron oxide  
26 nanoparticles (hybridosomes®) on the radiotherapy of glioblastoma, using murine GL261-  
27 Luc<sup>+</sup> brain tumor model. While iron oxide seems to have no beneficial effect for radiotherapy,  
28 we observe a real effect of gold nanoparticles —despite their low amount— with a median  
29 survival increase of almost 20% compared to radiotherapy only and even 33% compared to the  
30 control group. Cellular and *in vivo* studies show that a molecule of interest nano-precipitated in

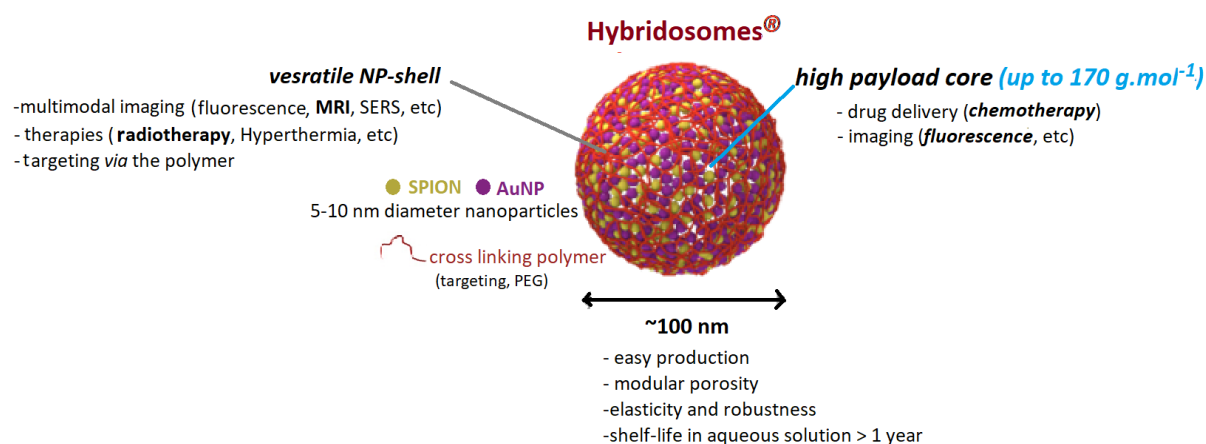
1 the core of the hybridosomes® is released and internalized by the surrounding brain cells.  
2 Finally, *in vivo* studies show that hybridosomes® injected intra-tumorally are still present in  
3 the vicinity of the brain tumor more than 5 days after injection (duration of the Stupp protocol's  
4 radiation treatment). Interestingly, one mouse treated with radiotherapy in the presence of gold-  
5 containing hybridosomes® survived 78 days. Monitoring of the tumoral growth of this long-  
6 term survivor using both MRI and bioluminescence revealed a decrease of the tumor size after  
7 treatment. These very encouraging results are a proof-of-concept that hybridosomes®, are  
8 really effective tools for combined therapies development (chemo-radiotherapy).

9

## 10 **Introduction**

11 Glioblastoma multiforme (GBM: WHO grade IV), with an incidence of 5 per 100,000 people,  
12 is the most common type of brain tumor. It is highly aggressive and often deeply infiltrates  
13 brain tissues<sup>1</sup>. Today, the standard treatment, defined as the Stupp protocol, is based on surgery  
14 followed by radiotherapy (5 times 2 Gy per week for 6 weeks; total 60 Gy) with concomitant  
15 (75 mg per square meter of body-surface area per day, 7 days per week from the first to the last  
16 day of radiotherapy) chemotherapy with temozolomide as adjuvant (150 to 200 mg per square  
17 meter for 5 days during each 28-day cycle)<sup>2</sup>. Despite this severe treatment, the median survival  
18 remains poor (< 18 months) with a rate of 5-year survival less than 5%<sup>3,4</sup>. GBM is one of the  
19 few cancers for which there has been little increase in life expectancy over the past 30 years. In  
20 addition to the infiltrating nature of the tumor, which makes total resection of the tumor by  
21 surgery almost impossible, one of the major obstacles to the treatment of GBM is the Blood  
22 Brain Barrier (BBB). Indeed, the BBB severely limits the penetration of chemotherapeutic  
23 molecules and radiosensibilizing agents into brain tumor tissues. Brain tumor development  
24 partly disturbs the permeability of this BBB but often at its latest stage and not uniformly, which  
25 leads to an inefficient drug delivery<sup>5</sup>. To overcome this limitation, one strategy is the use of  
26 local administration<sup>6</sup>. Thus, implantable polymer devices delivering a chemotherapy such as  
27 Gliadel® are presently used in the clinics. Direct intracranial delivery of drug-loaded vehicles,  
28 notably lipid nanocapsules, or of cellular vehicles such as stem cells producing growth factor  
29 inhibitors, has yielded promising results in orthotopic GBM models.<sup>7</sup> Alternatively, intracranial  
30 infusion of drugs through convection-enhanced delivery devices enables the administration of  
31 drugs over longer period and has shown encouraging results in small animal models (see  
32 reference<sup>8</sup> for review).

1 Among the numerous therapeutic strategies which have been explored <sup>9,10</sup>, an attractive lead  
2 with the promise of a breakthrough in cancer therapies is the improvement of radiotherapy  
3 through the use of radiosensitizing nanoparticles, in particular high-Z nanoparticles (Z: atomic  
4 number)<sup>11–14</sup>. Indeed, the use of conventional radiotherapy is limited by the damages caused to  
5 healthy tissues in the path of irradiation. In the presence of high-Z nanoparticles, the energy is  
6 absorbed and “deposited” much more locally than in normal tissues, due both to the strong  
7 photon absorption and to the conversion of the initially high energy radiation into several low  
8 energy Auger electrons. First, photon-X are absorbed by atoms *via* the photoelectric effect, with  
9 an efficiency roughly proportional to  $Z^4$ , thus favoring high-Z atoms in comparison to soft  
10 tissues. Following the absorption of a single photon of high energy, a high-Z atom may expel a  
11 dozen of Auger electrons of lower energy, hence of low penetration (~10 nm). Furthermore, the  
12 generated Auger electrons and secondary X-rays induce the production of hydroxyl radicals  
13 ( $\text{HO}\cdot$ ) *via* water radiolysis. These, and other reactive oxygen species (ROS) that are further  
14 generated readily react with biological molecules, including DNA, proteins and lipids inducing  
15 cell death<sup>15</sup>. Gold (Z=79) is a material of choice, since it combines the advantages of  
16 biocompatibility and strong photoelectric effect <sup>12</sup>. The first *in vivo* experimental evidences of  
17 the radiosensitization effect of gold nanoparticles (AuNP) dates back to the 2000s<sup>16,15</sup> and the  
18 number of reports has kept increasing since then. The location of the gold nanoparticles at the  
19 tumor site can be verified by computed tomography (CT). Among the other metal-based  
20 materials that have been considered for radiosensitization, gadolinium and superparamagnetic  
21 iron oxide have the advantage of being easily tracked by MR-imaging (MR: magnetic  
22 resonance)<sup>17</sup>.



23  
24 **Scheme:** Schematic representation of a hybridosome® summarizing its main physicochemical  
25 characteristics and its multiple and general theranostic potentialities in terms of therapies, imaging and  
26 targeting. The potentialities used in the present work are highlighted in bold.

1 Recently we have introduced a new type of multimodal nanocapsules, named hybridosomes®  
2 (H®), whose shell consists of inorganic nanoparticles (NP) crosslinked with a polymer<sup>18,19</sup>  
3 (Scheme). Interestingly, these nanocapsules are produced by a simple nanoprecipitation  
4 method, which allows at the same time the formation of the NP-shell and the encapsulation of  
5 a hydrophobic active ingredient. A previous study demonstrated that the storage capacity in the  
6 core of these nanocapsules is extremely high (over 170 g.L<sup>-1</sup>), the hydrophobic ingredient being  
7 condensed in a nanoprecipitated form<sup>20</sup>. Hybridosomes® containing iron oxide  
8 superparamagnetic nanoparticles (SPION), named hereafter H(Fe), can be used as MRI T<sub>2</sub>  
9 contrast agents, with an efficiency comparable to commercial iron oxide based contrast agents  
10 such as Feraspin XXL™<sup>18</sup>. In addition, a stealth-providing poly(ethylene glycol) block (PEG)  
11 can be added to the polymer holding the shell, to limit uptake by monocytes and delay their  
12 sequestration in the specialized organs of the immune system. Based on these results,  
13 hybridosomes® appear to be prime candidates for the treatment of cancers requiring  
14 multimodal therapies, such as glioblastoma.

15 The main aim of the present work is to evaluate the radiosensitizing effect of H(Fe;Au)  
16 hybridosomes® composed of superparamagnetic iron oxide and a small amount of gold  
17 nanoparticles (10%) on GBM after intratumoral injection in mice implanted with the GL261  
18 brain tumor model. We first evaluated the distribution of hybridosomes® *in vitro* and *in vivo*.  
19 We took advantage of iron oxide NP to follow the *in vivo* biodistribution of H(Fe;Au) using  
20 MRI and to evaluate their presence in post-mortem tissues by histology (Perls staining). Then,  
21 we performed a survival study to evaluate the increased therapeutic effect of H(Fe;Au) in  
22 combination with irradiation. Six groups of mice were examined, including 3 groups not treated  
23 with radiotherapy (injected with H(Fe), H(Fe;Au) or none) and 3 similar groups receiving  
24 radiotherapy. Tumor growth was monitored in all groups by both bioluminescence and MRI.  
25 We have also characterized the transfer of an encapsulated charge from hybridosomes® to  
26 tumor cells, *in vivo* and *in vitro*, using a fluorescent dye BODIPY as a model. All these works  
27 and the good results obtained, allow us to consider the use of hybridosomes® as a unique  
28 theranostic nanoplatform to efficiently combine chemo- and radiotherapy, offering the  
29 possibility of a follow-up by imaging.

## 30 **Materials and methods**

### 31 *Elaboration and characterization of hybridosomes®*

32 Poly(ethylene glycol)-*b*-Poly(acrylic acid) (PEG-PAA) (M<sub>PEG</sub> = 2 kg.mol<sup>-1</sup>; M<sub>PAA</sub> = 7.2  
33 kg.mol<sup>-1</sup>) was kindly provided by Dr G. Casterou. Tetrahydrofuran (THF, GPR Rectapur ≥99%

1 stabilized) was purchased from VWR and used as received. Samples were made using MilliQ  
2 water ( $18.2 \text{ M}\Omega\cdot\text{cm}^{-1}$ ). The fluorescent dye 4,4-difluoro-8-(4-trimethylsilylethynylphenyl)-  
3 1,3,5,7-tetramethyl-2,6-diethyl-4-bora-3a,4a-diaza-s-indacene (BODIPY,  $M = 476.2 \text{ g}\cdot\text{mol}^{-1}$ )  
4 was kindly provided by Dr O. Mongin (Univ Rennes, CNRS, ISCR-UMR6226, F-35000  
5 Rennes, France.)<sup>21</sup>.

6 The iron oxide ( $\gamma\text{-Fe}_2\text{O}_3$ ) nanoparticles (SPION) were synthesized following a reported  
7 procedure with slight modifications<sup>22</sup>. Briefly, the SPION are obtained *via* hydrolysis of an  
8 organometallic Fe(II) precursor in the presence of a stabilizing ligand (here 2 eq. of octylamine  
9 and 1 eq. of oleic acid, relative to Fe), in the absence of any other solvent. Oleylamine-coated  
10 gold NP were synthesized following the procedure reported by Liu *et al.*<sup>23</sup>. Briefly, AuNP were  
11 synthesized in oleylamine, which acts both as a reductor of the gold salt ( $\text{HAuCl}_4, 3 \text{ H}_2\text{O}$ ) at  
12  $150^\circ\text{C}$  and as a capping agent to stabilize the newly synthesized NP. After 1h30 of reaction,  
13 AuNP are readily dispersed in THF after precipitation in ethanol and centrifugation. Note that  
14 it is important for the elaboration of hybridosomes® to use alkyl-coated (hydrophobic) NP.

15 The magnetic hybridosomes® H(Fe) and H(Fe;Au) were prepared by rapidly adding water to a  
16 THF solution containing the iron oxide NP (plus the AuNP for H(Fe;Au)), in order to reach a  
17 water/THF composition of 75/25 v/v. Mixing was promptly followed by a very quick vortexing.  
18 After ca 7 h, PEG-PAA ([acrylic acid units] =  $2.4 \text{ mmol}\cdot\text{L}^{-1}$ ) was added to the mixture and  
19 the solvent was slowly evaporated overnight at  $40^\circ\text{C}$ . Two 24 h magnetic separations were  
20 performed using a permanent magnet, and the pellets were dispersed in fresh water to recover  
21 the purified hybridosomes®. To elaborate dye-loaded hybridosomes®, the BODIPY was  
22 dissolved in the THF solution in order to reach a final dye concentration in the water/THF  
23 mixture of  $50 \mu\text{mol}\cdot\text{L}^{-1}$ . After encapsulation, the BODIPY-loaded hybridosomes® can be  
24 excited at 488 nm, which is close to their maximum of absorbance, to produce a broad band  
25 emission around 550 nm<sup>20</sup>. The distribution of hydrodynamic diameters and H® concentration  
26 was determined by Nanoparticle Tracking Analysis (NTA), using a Nanosight LM10 device  
27 system (Malvern Panalytical) equipped with a 40 mW laser working at  $\lambda = 638 \text{ nm}$ . Video  
28 sequences were recorded *via* a CCD camera operating at 30 frames per second and evaluated  
29 via the NANOSIGHT NTA 2.0 Analytical Software Suite. For each sample, 3 acquisitions with  
30 an acquisition time of 60 s were performed at  $25^\circ\text{C}$ . TEM analysis was performed using a Jeol  
31 1400 electron microscope equipped with a Gatan Orius 1000 camera. The elemental  
32 concentrations of iron ( $18.7 \mu\text{g}/\text{mL}$ ) and gold ( $2 \mu\text{g}/\text{mL}$ ; in the case of H(Fe;Au)) in the purified  
33 H® suspensions were determined by atomic spectroscopy. Typically, the H® were dissolved  
34 in nitric acid for one week under heating at  $40^\circ\text{C}$ . After appropriate dilution with milliQ water,

1 the concentrations were determined using an iCAP 7000Series ICP-OES spectrometer (Thermo  
2 Scientific) under an argon flow.

3

#### 4 *Tumoral cells, mice and brain implantation*

5 GL261-Luc<sup>+</sup> cells were kindly provided by R. Hashizume (University of California, San  
6 Francisco, CA).<sup>24</sup> Cells were cultured in DMEM medium (Dutscher, Brumath, France)  
7 supplemented with 10 % heat inactivated FBS (Dutscher) and 2 mM L-Glutamine (PanBiotech,  
8 Aidenbach, Bavaria, Germany).

9 C57BL/6 (B6/Rj) and C57BL/6 albino (B6/Rj-Tyrc/c) mice were purchased from Janvier Labs  
10 (Saint Berthevin, France) and bred in the animal facility of the University of Rennes (ARCHE,  
11 Biosit, SFR UMS CNRS 3480-INSERM 018, Université de Rennes 1) under specific pathogen-  
12 free status. Mice were used at 6–12 weeks of age and manipulated according to institutional  
13 guidelines.

14 For stereotaxic implantation, mice were anesthetized with an intraperitoneal injection of  
15 ketamine (10 µg/g) and xylazine (1 µg/g) and were placed in a stereotactic frame (Stoelting,  
16 Dublin, Ireland). The animals underwent an injection (0.5 µL/min) of 10.10<sup>3</sup> GL261-Luc<sup>+</sup> cells  
17 in 2 µL sterile PBS with a Hamilton syringe, at the level of the bregma 3 mm on the right of the  
18 medial suture and at a depth of 2.5 mm. The syringe was held in place for an additional minute  
19 and was slowly removed to avoid backfilling of the solution.

20 The protocols were approved by the French Ministère de l'Enseignement Supérieur et de la  
21 Recherche and by the local Ethic Committee (Comité Rennais d'Ethique en matière  
22 d'Expérimentation Animale (CREEA) (France) (Agreement # 10972)). In particular, the  
23 number of animals per study group was validated and therefore allowing not to multiply the  
24 number of tumor models.

25 The mice were daily observed and were euthanized when showing specific clinical signs,  
26 following standard procedures. Among the conventional signs, those that were observed are the  
27 following:

28 **Notable Clinical Signs** (limit point reached if 3 simultaneous signs are detected):  
29 agitation/aggressiveness; hypomotility/hyporeactivity; moderate incoordination; stereotypes;  
30 generalized muscle flaccidity; abdominal swelling; arched back; weight loss less than 10 %, no  
31 food intake for less than 2 days.

32 **Severe Clinical Signs** (limit point reached if 1 sign is detected): akinesia; decubitus;  
33 difficulty/impossibility of mobilization; marked incoordination; generalized tremors;  
34 convulsions; weight loss more than 10%; no food intake for more than 2 days.

1  
2  
3  
4  
5  
6  
7  
8  
9  
10  
11  
12  
13  
14  
15  
16  
17  
18  
19  
20  
21  
22  
23  
24  
25  
26  
27  
28  
29  
30  
31  
32  
33  
34

### *Hybridosomes® injection and irradiation protocol*

For *in vivo* distribution, dye-loaded H(Fe;Au) were injected in the brain tumor of mice 14 days after implantation of the GL261-Luc<sup>+</sup> tumor cells. For assessment of the irradiation procedure, H(Fe) were injected in the tumor to groups 2 & 5 and H(Fe;Au) to groups 3 & 6, at day 14 or 16 (albino mice) after tumor cells injection, and radiotherapy started the same day for groups 4, 5 & 6, as indicated in Table 1. The albino (a) and non-albino (na) mice were distributed within the groups as follows: group 1 = 6(a)/5(na); group 2 = 7(a); group 3 = 3(a)/6(na); group 4 = 6(a)/6(na); group 5 = 11(a); group 6 = 7(a)/6(na). The injected amount is 5  $\mu\text{L}$  of a concentrated dispersion of hybridosomes® in PBS ( $500 \mu\text{g}\cdot\text{mL}^{-1}$  Fe and  $53 \mu\text{g}\cdot\text{mL}^{-1}$  Au in the case of H(Fe;Au), i.e. ca 125  $\mu\text{g}$  Fe & 13  $\mu\text{g}$  Au/mouse kg. The intratumoral injection is performed as described above at the rate of  $1 \mu\text{L}\cdot\text{min}^{-1}$  at the exact same location as tumor implantation. For tumor irradiation mice were anesthetized with isoflurane. Irradiation was performed using an X-ray generator (CellRad, Faxitron Bioptics, Tucson, AZ)) on the head area at 2 Gy/day for 5 days.

### *Confocal microscopy*

Images were acquired using a LSM 880 confocal microscope (Zeiss, Oberkochen, Deutschland) equipped with a 63X oil-immersion objective (NA 1.4) and driven by ZEN software. The beam excitation laser was 488 nm and the emission channel detector was set at 517-544 nm. Images were analyzed and processed with ImageJ.<sup>25</sup>

### *Tissue isolation and Histology*

After collection, brains, livers, cervical lymph nodes and spleens were frozen in isopentane (Sigma-Aldrich, St Louis, MO) and serially sectioned at 10  $\mu\text{m}$  using a Leica cryostat (Leica, Solms, Germany) at  $-30^\circ\text{C}$ . Slides were firstly scanned using the NanoZoomer 2.0 HT (Hamamatsu Photonics K.K., Hamamatsu, Japan) for hybridosomes® fluorescence acquisition. Then, slices were stained either with DAPI (SouthernBiotech, Birmingham, AL), Hematoxylin and eosin (H&S) and/or Perls (specific iron staining) before second acquisition.

### *In vivo Bioluminescence assays*

Mice received an intraperitoneal injection of 150  $\mu\text{L}$  of  $15 \mu\text{g}\cdot\mu\text{L}^{-1}$  D-Luciferin K<sup>+</sup> solution, (Interchim, Montluçon, France) while anesthetized via inhaled isoflurane and monitored using a Photon imager (Biospace Lab, Nesles la Vallée, France) equipped with a highly sensitive

1 cooled CCD camera. Data were analyzed using the cpm (count per minutes) per cm<sup>2</sup> focused  
2 on the head.

3

#### 4 *In vivo Magnetic Resonance Imaging*

5 *In vivo* Magnetic Resonance Imaging (MRI) experiments were carried out at 4.7 Tesla with a  
6 horizontal Biospec 47/40 imaging system (Bruker Biospin, Wissembourg, France). After prior  
7 anesthesia with isoflurane, mice were placed in a prone position and held in a contention system  
8 equipped with a face mask for anesthesia with 1-2.5% isoflurane in air. Breathing was  
9 monitored with a pneumatic probe. The body temperature was maintained at 36.5-37.5°C by a  
10 feedback-regulated heating pad throughout the imaging protocol. Tumor size was monitored  
11 using axial and coronal T2-weighted images obtained using a Rapid Acquisition with  
12 Relaxation Enhancement (RARE) sequence <sup>26</sup>. Acquisition parameters were as follows:  
13 TR = 3500 ms; TE/TEeff = 9.35/28.5 ms; RARE factor = 8; 2 averages, in plane  
14 resolution = 100 μm x 100 μm, slices thickness = 1 mm. Acquisition time was 2 min 20 s for  
15 each acquisition.

16 Tumor volumes V (mm<sup>3</sup>) were calculated according to the formula,  $V = (L \times l \times h) \times \pi/6$ , with  
17 L, l and h the lengths of the 3 main axes of the tumor measured on axial and coronal MR Images.

18

#### 19 *Statistical analysis*

20 To avoid tumor size bias, the mice were distributed into 6 groups such that each mice group  
21 contains tumors of all sizes, based on MRI measurements at days 9/10 after tumor implantation  
22 (see Figure SI-1). Two mice (out of 54) with tumor size exceeding 30 mm<sup>3</sup> were excluded from  
23 the cohort, after which the mean diameter size was  $4.8 \pm 1.12$  mm<sup>3</sup>.

24 Data are expressed as median survival and were analyzed using GraphPad Prism 7.0 (GraphPad  
25 Software, Inc., San Diego, CA) or Origin softwares. The P-values were calculated using the  
26 Logrank (Mantel-Cox) test (\*p<0.05).

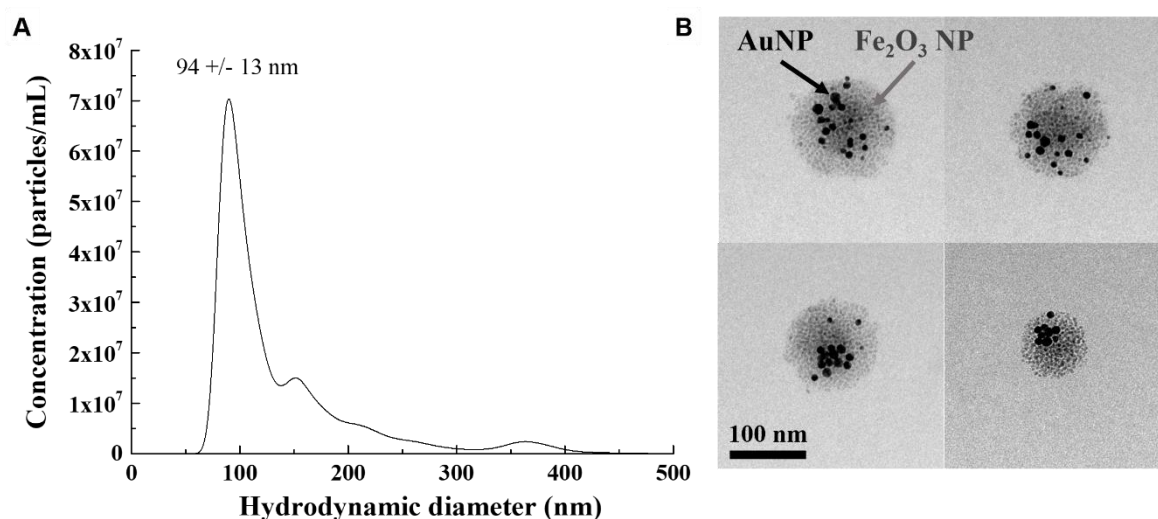
27

## 1 Results

2

### 3 Characterization of the gold containing hybridosomes® H(Fe;Au).

4 As already described in detail previously elsewhere<sup>18,27</sup>, our hybridosomes® are very original  
5 types of nanocapsules (Scheme). They are original both in *i*) their synthesis (simple and fast),  
6 *ii*) their composition (inorganic NP, organic polymer) and *iii*) their multifunctionality, coming  
7 from the NP shell (imaging, therapy) as well as from the core allowing the loading of a large  
8 number of molecules (efficient drug delivery). In this work, we have optimized the shell of our  
9 magnetic iron-oxide hybridosomes(R), usually only made of SPION, by adding a small number  
10 of gold nanoparticles (AuNP) in order to confer a radiosensitization property to our  
11 nanocapsules. The designed mixed iron-gold hybridosomes® H(Fe;Au) were characterized by  
12 transmission electron microscopy (TEM) and single Nanoparticle Tracking Analysis (NTA)  
13 (Figure 1A). The size distribution measured by NTA in aqueous suspensions shows a main  
14 mode of the hydrodynamic diameter at  $94 \pm 13$  nm. The TEM analysis of the suspensions dried  
15 on a TEM grid confirms the formation of capsules of  $\sim 100$  nm, containing both gold and iron  
16 oxide NP. Single AuNP (diameter  $9.8 \pm 2.3$  nm) are larger than single iron oxide NP (diameter  
17  $4.2 \pm 1.7$  nm) and appear with a darker contrast, since TEM contrast increases with electron  
18 density ( $Z_{\text{Au}} = 79$ ,  $Z_{\text{Fe}} = 26$ ,  $Z_{\text{O}} = 8$ ). A final Fe:Au composition of ca 10:1 was determined using  
19 ICP-EOS titration.



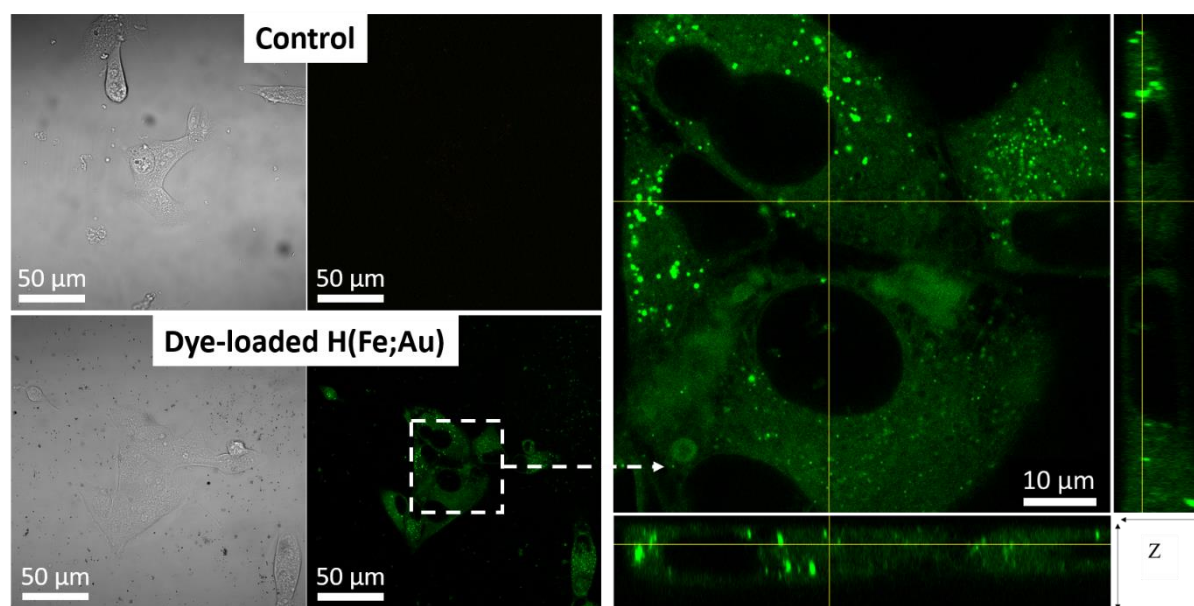
20

21 **Figure 1 :** Hybridosomes® characterization. (A) Single Nanoparticle Tracking Analysis of a water-  
22 suspension of H(Fe;Au). (B) Transmission electron micrographs of H(Fe;Au) with arrows indicating  
23 AuNP (black) and Fe<sub>2</sub>O<sub>3</sub> NP (grey). The mass ratio Fe:Au is ca 10:1.

24

25 **Intracellular delivery of encapsulated payload.**

1 In a recent study, we developed the process of encapsulation in hybridosomes®, using a  
2 fluorescent model dye (BODIPY) and iron oxide hybridosomes®<sup>20</sup>. The dye is encapsulated  
3 in a solid form (nanoprecipitate) with two main emission bands centered at 560 nm (green) and  
4 625 nm (red). Here, we investigated the release of the encapsulated dye from the gold  
5 containing H(Fe;Au) into GBM cells. To this aim, GL261-Luc<sup>+</sup> cells were incubated for 2 hours  
6 with BODIPY-loaded H(Fe;Au) and then analyzed by confocal microscopy. As seen in Figure  
7 2, the green fluorescence of the dye was detected in the cytosol of incubated cells, but not in  
8 the nucleus.

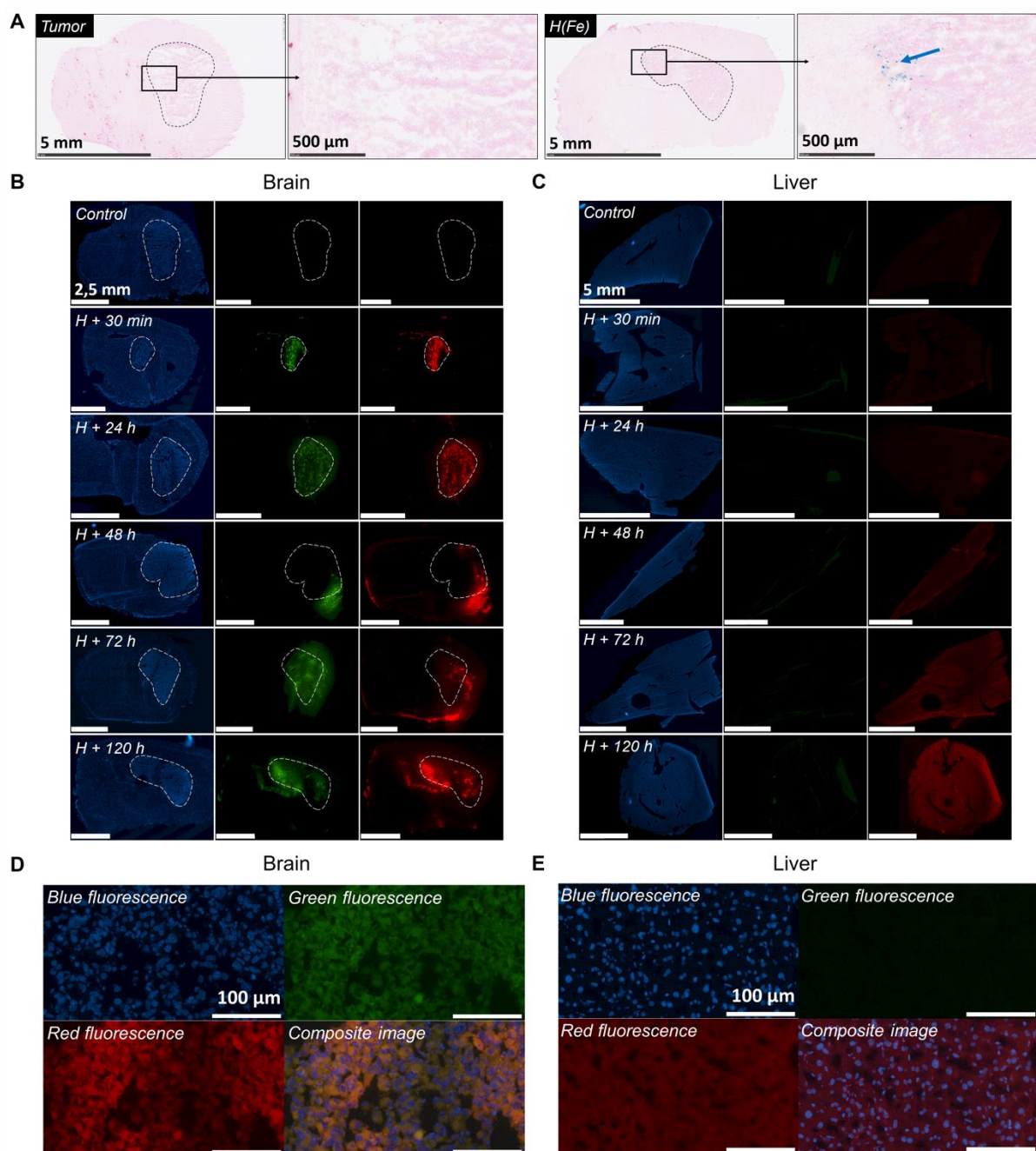


10 **Figure 2** – Left: Bright-field image and confocal fluorescence microscopy of unstained GL261 cells  
11 after incubation with dye-loaded H(Fe;Au), showing diffusion of the dye in the cytosol but not in the  
12 nucleus. Right: enlargement and Z-scan. Imaged for the BODIPY green fluorescence.

### 14 **Biodistribution of the hybridosomes® and of their cargo**

15 We next sought to evaluate the *in vivo* biodistribution of the capsule and cargo (i.e. encapsulated  
16 load) after intra-tumoral injection of dye-loaded hybridosomes®. To this aim, BODIPY-loaded  
17 H(Fe), were injected in the brain tumors of 10 mice, 14 days after implantation of the  
18 GL261 - Luc<sup>+</sup> tumor cells. Two mice were sacrificed 30 min after injection, and then every day  
19 to study their main organs. The presence of iron (more precisely Fe<sup>3+</sup> ions) from the shells of  
20 the hybridosomes® was assessed by optical microscopy following Perls staining on slices of  
21 brains and livers at day 5 (Figure 3A). In brain slices, iron is irregularly present near the edges  
22 of the tumor. No significant accumulation of exogenous iron could be detected in the liver.  
23 The BODIPY fluorescence (green + red) from slices of brain, liver, spleen and cervical lymph  
24 nodes is displayed in Figure 3B & 3C (brain and liver) and Figure SI- 2 (spleen and cervical

1 lymph nodes). No signal was detected for non-injected mice (upper pictures). For injected mice,  
2 30 min after injection, the fluorescence of the BODIPY remains localized in a limited area,  
3 most probably surrounding the site of injection (Figure 3B). Then, it spreads spatially over the  
4 5 days of monitoring. Interestingly, the fluorescence signal seems to co-localize with the tumor  
5 (with the exception of the individual analyzed at 48 h). Some diffuse fluorescence also appears  
6 in the liver, but with a delay of a few days. A low amount of fluorescence is also significant in  
7 the cervical lymph nodes after a few days but remains non-significant in the spleen (Figure SI-  
8 2).



9  
10 **Figure 3** – Presence of iron in the tumor, and release of encapsulated dye (BODIPY), emitting in the  
11 red and green, in the brain and liver after intratumoral injection of BODIPY-loaded H(Fe) in mice with

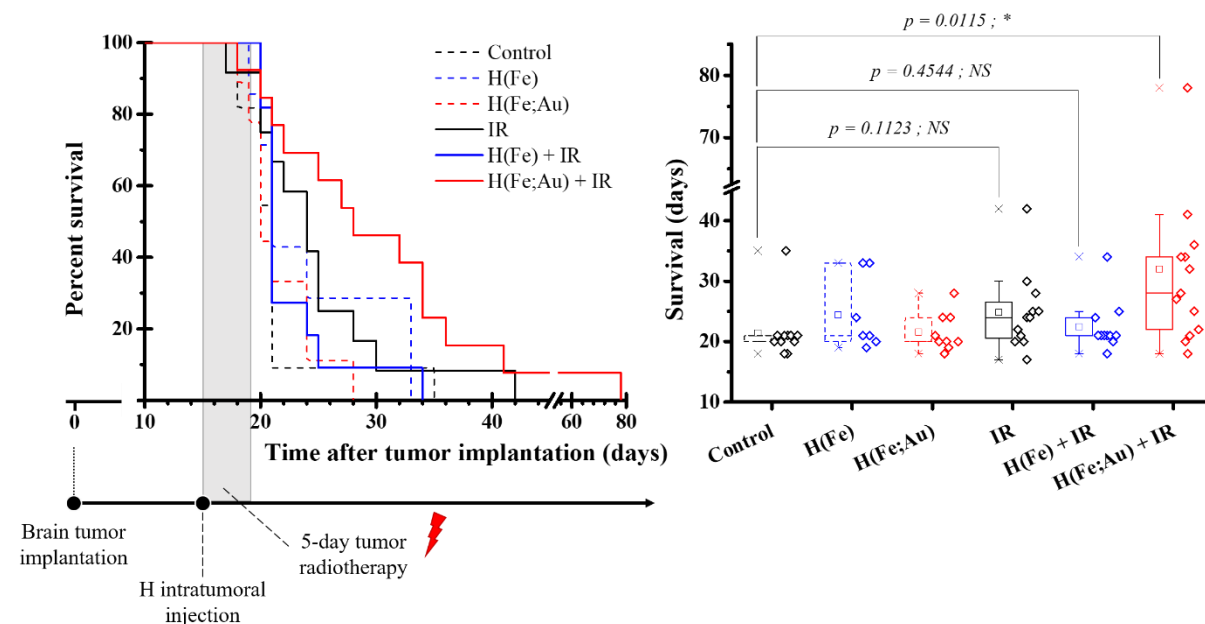
1 GL261 brain tumor. (A) Optical microscopy images with HES/Perls stained sections of tumoral brain 5  
2 days after the injection, showing distribution of the iron from the hybridosomes® shell. Pictures show  
3 representative results (left: non-injected; right: injection of BODIPY loaded-H(Fe)). The blue arrow  
4 indicates the localization of iron (blue staining). (B) & (C) Fluorescence imaging: brain and liver slices  
5 were stained with DAPI and imaged for DAPI (blue) and BODIPY (green+red) fluorescence. Dash  
6 lines: tumor area. (D) & (E) Enlargements of (B) and (C), respectively, at day 5. The images show that  
7 the dye is released in the cytosol.  
8

## 9 **Survival**

10 We sought to assess whether hybridosomes® containing a small amount of AuNP (H 90% Fe;  
11 10% Au) could potentiate the therapeutic effect of radiations on GL261-Luc<sup>+</sup> brain tumor  
12 model. To this aim, GL261-Luc<sup>+</sup> brain tumor-bearing mice were divided into six groups with  
13 similar tumor size distributions (Figure SI-1), as measured by MRI 9 or 10 days after tumor  
14 implantation. The mice received intratumoral injection of either H(Fe;Au), H(Fe) or none,  
15 depending on their group, as shown in Table 1. The same day, radiotherapy started for the  
16 groups concerned. Radiotherapy was applied for 5 days with 2 Gy / day. Figure 4 shows the  
17 Kaplan-Meier survival curves for all groups.  
18

19 **Table 1** – Description of the different mice groups and the associated treatments.

<b>Group treatment</b>	<b>Number of mice</b>
<b>Group 1:</b> <i>tumor – no treatment (control)</i>	12
<b>Group 2:</b> <i>tumor + H(Fe)</i>	8
<b>Group 3:</b> <i>tumor + H(Fe;Au)</i>	9
<b>Group 4:</b> <i>tumor + radiotherapy</i>	12
<b>Group 5:</b> <i>tumor + H(Fe) + radiotherapy</i>	11
<b>Group 6:</b> <i>tumor + H(Fe;Au) + radiotherapy</i>	13



1  
2 **Figure 4** – Kaplan-Meier curves (left) and box plot representation (right) of mice survival with GL261  
3 gliomas after treatment with radiotherapy and/or hybridosomes®. Intratumoral injection of H(Fe) (blue),  
4 H(Fe;Au) (red) or none (black) was achieved two weeks after the implantation of GL261-Luc+ cells,  
5 and irradiation started immediately with 2 Gy per day for 5 days (full lines: irradiated; dashed lines:  
6 non-irradiated). P values were calculated by the log-rank test. IR=irradiation.

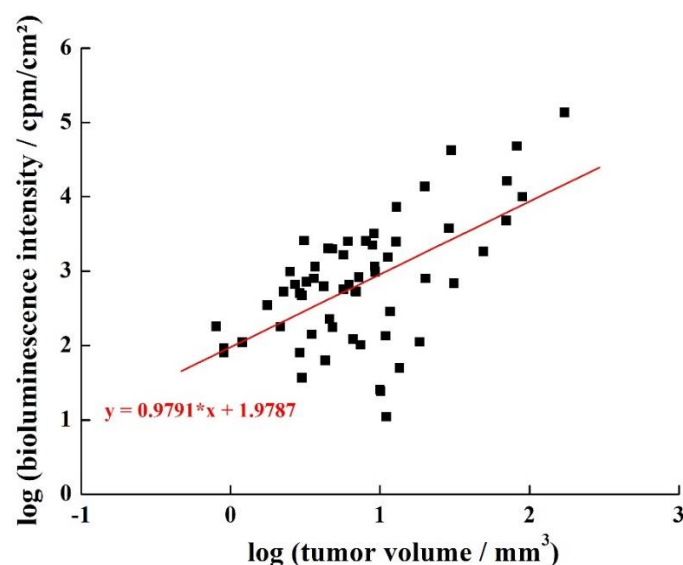
7 The Figure 4 shows that the group of mice treated with H(Fe;Au) combined with irradiation  
8 (red full line) exhibit the longest median survival (28 days), far ahead of other groups which  
9 have a median survival in between 21 days (untreated mice) and 24 days (radiotherapy only).  
10 More precisely, survival was significantly increased in the H(Fe;Au) + irradiation group  
11 compared to untreated mice (\* $p = 0.0115$ , logrank). In contrast, even if the number of mice  
12 used was almost the same (12 and 13 respectively), treatment with irradiation showed no  
13 significant benefit ( $p=0.1123$ ). The groups treated with H(Fe), H(Fe;Au) and even  
14 H(Fe)+irradiation showed no significant difference with the control group receiving no  
15 treatment.

### 17 Monitoring of the tumoral growth by Bioluminescence and MRI

18 The first bioluminescence measurement was achieved on day 9 after tumor cells implantation,  
19 and days 10 or 11 for MRI. No measurements were achieved during the irradiation period (until  
20 day 21) to avoid repetitive anesthesia. Then, measurements were acquired every 4-5 days until  
21 death. Only albino mice could be followed by bioluminescence. All measurements are  
22 presented in Figure SI- 4. Whereas the survival of mice belonging to the 3 non-irradiated groups  
23 (#1-3) rarely exceeded the irradiation period (only 2 mice out of 18), it is clear from  
24 bioluminescence measurements that in the groups receiving irradiation (groups 4-6) several

1 individuals exhibited a reduction in signal intensity after the irradiation period. This is  
2 particularly true in group 6 (H(Fe;Au) + irradiation) where 3 out of 7 mice showed a significant  
3 decrease of bioluminescence after irradiation. The case of one particular mouse who survived  
4 for 78 days is detailed in the following section. In the control group 4, irradiated but receiving  
5 no hybridosomes®, only 1 out of 6 mice underwent such signal decrease. Two mice in the  
6 group irradiated in the presence of H(Fe) (group 5) had a temporary stop of tumor growth, but  
7 no decrease in size was observed.

8



9

10 **Figure 5** – Log-Log representation of the bioluminescence intensity vs MRI measurement of tumor  
11 volume, for albino mice over the survey.

12 Bioluminescence and MRI are complementary techniques for the monitoring of tumor growth.  
13 Bioluminescence provides a measurement of the activity of the tumoral cells. It is rapid and  
14 cost-effective, but cannot be applied in the clinics. MRI is an imaging technique giving detailed  
15 morphological information on the tumor. However, the distinction between inflammation and  
16 tumor itself is not always straightforward. Since few studies present MRI and bioluminescence  
17 data simultaneously, we took advantage of this large set of data to check the correlation between  
18 MRI and bioluminescence measurements. Figure 5 shows a Log-Log representation of  
19 bioluminescence intensity vs tumor volume measured from MRI. It appears that the data follow  
20 roughly a straight line of slope 1, which indicates that the volume (from MRI) is positively  
21 correlated to bioluminescence intensity. The discrepancy is more important for small tumor  
22 volumes ( $< 10 \text{ mm}^3$ ). This might be due to the hyposignal of the iron oxide NP, masking the  
23 tumor contrast.

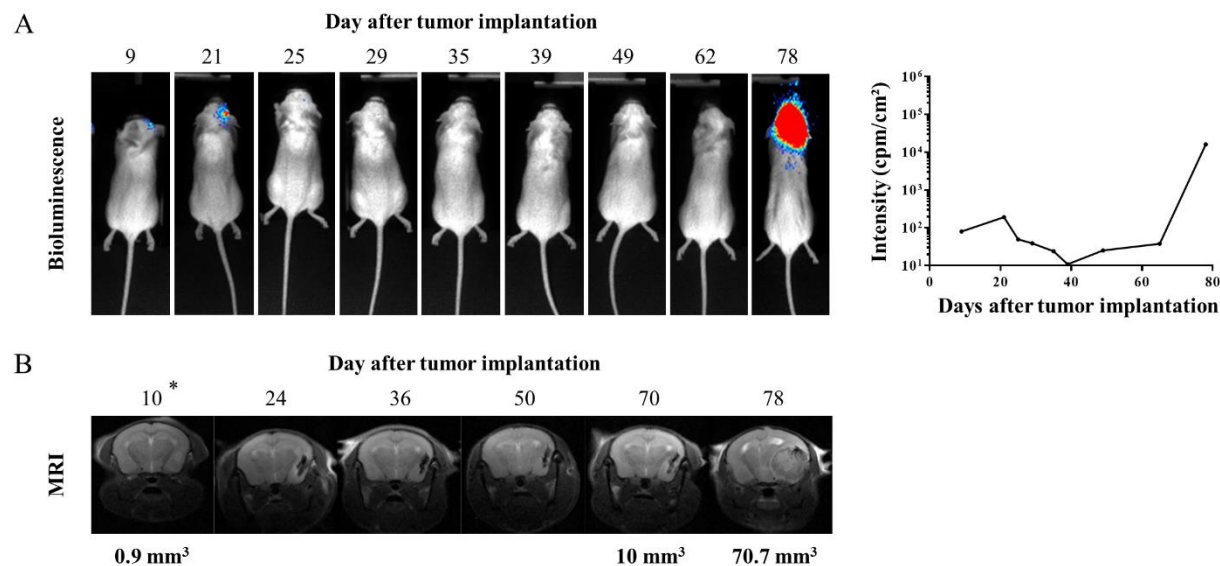
24

## 1 Case study of a long term survivor treated by radiotherapy combined with H(Fe;Au)

2 Of note, one mouse (#1082) treated with H(Fe;Au) combined with irradiation survived until  
3 day 78 after tumor implantation (Figure 4). Its tumor size was monitored over all this period by  
4 both bioluminescence and MRI. The bioluminescence signal (Figure 6A) from the GL261-Luc+  
5 implanted tumor clearly decreased after the irradiation treatment, over a period of almost three  
6 weeks (from day 21 to day 39). The decrease in intensity over this period is more than a factor  
7 of 20. From day 40, the bioluminescence increased again, first slowly, then abruptly. The tumor  
8 size was also monitored using MRI (Figure 6B). From day 24 to day 62 the tumor remained  
9 extremely small and hindered by the hypointense signal of the iron-oxide NP. A sudden burst  
10 of the tumor growth occurred in-between days 70 and 78.

11 To go further, the brain of the mouse # 1082 was collected after death, serially sectioned (every  
12 100  $\mu\text{m}$ ) and analyzed by optical microscopy after HES and Perls staining (Figure SI-3). A  
13 large tumor is clearly visible on HES stained slices, consistently with MRI and bioluminescence  
14 observations. Moreover, at day 78, Perls staining confirms the localization of iron at the upper  
15 edge of the tumor, as seen by MRI. It also confirms that iron from the H(Fe;Au) is still present  
16 even two months after intratumoral injection.

17



18

19 **Figure 6** – Case study. At day 14 after brain implantation of GL261-Luc+ cells, the mouse 1082  
20 underwent intratumoral injection of H(Fe;Au) and was treated by irradiation for one week.  
21 (A) Bioluminescence signal from the GL261-Luc+ tumor. (B) MRI of the brain. Day 10 is before  
22 injection of hybridosomes®, all other images are after injection of the hybridosomes® and show the  
23 hypointense signal from the magnetic iron-oxide NP.

24

## 25 Discussion

1 The results presented here suggest that the H(Fe;Au) efficiently potentialize the  
2 radiosensitization of GBM.

3 For these investigations, we used the GL261 model in immunocompetent mice considered as  
4 the standard model for glioblastoma research<sup>28</sup>. Indeed, despite some distinct features from  
5 spontaneous glioblastoma, notably the lack of characteristic histological vascularity, it shows  
6 rapid development and excellent reproducibility<sup>28</sup>. The nano-objects that are under  
7 investigation here have the potential to provide radiosensitization and encapsulate a  
8 chemotherapy at the same time.

9

10 *Hybridosome® should be considered for the release of a chemotherapy.*

11 The standard treatment for glioblastoma is a combination of chemotherapy and external  
12 radiation therapy. In this context, we are interested in developing and characterizing the  
13 capacity of hybridosomes to combine concomitant radiotherapy and chemotherapy. Thus, in  
14 the work presented here, we wanted to characterize the ability of our hybridosomes to deliver  
15 a molecule of interest to the tumor site of injection and to evaluate its fate (residence time,  
16 circulation). For this proof of concept, we have first used hybridosomes® loaded with a  
17 fluorescent dye to model the release of a drug in the tumor environment.<sup>29</sup> The *in vivo*  
18 fluorescence analysis of the brain shows that the dye-loaded hybridosomes® release their  
19 payload throughout the tumor area after intratumoral injection. The dye is present at least for 5  
20 days after injection. The model dye also accumulates into the liver, with some delay. A possible  
21 explanation for the emission observed in the liver, is that a fraction of dye-loaded  
22 hybridosomes® extravasate from the tumor site into the vascular system, where they are taken-  
23 up by the monocytes and conveyed to the liver. Indeed, since the hybridosomes® are ca 90 nm  
24 in diameter, they ought to be rapidly sequestered by the mononuclear phagocyte system (MPS)  
25 if they enter the bloodstream. Over this period of time, some dye also reaches the spleen and  
26 possibly the cervical lymph nodes. At the cellular level, we observed *in vitro* that the dye is  
27 able to diffuse into the cytosol of GL261 cells after incubation with dye-loaded H(Fe;Au), but  
28 also *in vivo* in the brain tumor area (cf. Figure 3D). The diffusion of the fluorescent BODIPY  
29 in the cytosol but not in the nucleus is consistent with previous fluorescence microscopy  
30 observations using a variety of encapsulated BODIPY dyes<sup>30</sup>. Since the capsule shell remains  
31 out of the cell<sup>20,30</sup>, the subcellular repartition of the encapsulated cargo depends only on its  
32 molecular properties. Thus, a specific drug may be able to enter the nucleus whereas our model  
33 dye does not. Altogether, these results are consistent with previous results, both *in vitro* and *in*

1 *in vivo*, showing that the iron-oxide hybridosomes® have a porous structure enabling the release  
2 of their payload in lipophilic compartments<sup>20,27</sup>.

3  
4 *H(Fe;Au)* significantly increase survival of brain tumor bearing mice treated by irradiation, at  
5 very low amount of gold content. Our main objective was to evaluate the *in vivo*  
6 radiosensitization effect of hybridosomes®, containing gold in small amounts. Our results show  
7 that the nanocapsules H(Fe) or H(Fe;Au) do not increase survival nor cause a tumor growth  
8 inhibition, when they are not associated with irradiation. Importantly, they also did not induce  
9 any toxicity. Very interestingly, the group receiving H(Fe;Au) combined with radiotherapy  
10 shows a significantly prolonged survival (28 days compared to 21 for the control group,  
11 \**p*=0.0115), whereas all other groups did not. In addition, it is also the only group for which  
12 bioluminescence intensity show a clear decay, for 3 mice over 7. One mouse of this group even  
13 showed a 78-days survival. This shows that the presence of gold is indispensable to achieve a  
14 beneficial effect.

15 Interestingly enough, the increase in survival rate was achieved here with very low amounts of  
16 gold. An early work<sup>31</sup>, based on numerical simulations, reported that an intratumoral  
17 concentration of 0.7% by weight wt/wt (i.e. 7 mg Au/g tumor) is required for a twofold dose  
18 enhancement using 140 kVp X-rays. Another numerical study suggested that a gold  
19 nanoparticle concentration of at least 0.1% is necessary to generate radiosensitization using  
20 low-energy X-rays (~100 keV)<sup>32</sup>. Most *in vivo* experimental studies obtained significant  
21 improvements in the survival of animals using gold nanoparticles in the range of 0.1-75 mg/g  
22 tumor<sup>11,15,31</sup>. It is important to note that in the case of intravenous injection, these quantities are  
23 determined by postmortem gold titration in the tissues. However, the proportion of  
24 nanoparticles having reached the tumor is generally less than 1%, which may lead to injecting  
25 doses that are beyond reasonable for clinical translation<sup>33</sup>. Roux *et al.* estimated that an  
26 injection of 8 µg/g (body weight) or less is relevant for clinical translation. Since then, some  
27 significant radiosensitizing effects were observed with gold nanoparticles at less than 5 µg/g<sup>34-</sup>  
28<sup>36</sup>. In the present study, mice were injected 0.25 µg of Au, or approximately 0.01 µg/g (body  
29 weight) associated with irradiation in the range ~ 10-100 keV, as in most reported preclinical  
30 studies. Therefore, there is an opportunity to increase the amount of gold to increase the  
31 radiotherapeutic benefit. This can be easily achieved without increasing the total amount of  
32 hybridosomes® by increasing the ratio of gold to iron oxide NP in their shell or even using pure  
33 gold hybridosomes®. Indeed, iron oxide was used here as a mean to assess the presence of the  
34 hybridosomes® at the site of injection. However, in the case of surgical application, this might

1 not be necessary. Note that despite the fact that the radiation enhancement is expected to be  
2 much lower at clinical radiation energies (MeV), many reports show that high-Z materials such  
3 as gold and gadolinium still have a significant dose deposition effect <sup>11,13,37</sup>.

4  
5 *Iron oxide show no radiosensitization effect.* It is important to note that H(Fe) did not potentiate  
6 the radiotherapy, and even possibly induced a slight deleterious effect compared to radiotherapy  
7 alone. Indeed, it contrasts with a few previous studies reporting a radiosensitization effect of  
8 iron oxide nanoparticles.<sup>38,39</sup> This effect is not primarily related to the increase in dose  
9 deposition, as in the case of gold, but results from the iron-catalyzed production of reactive  
10 oxygen species (ROS) *via* the Fenton or Haber-Weiss reactions <sup>14</sup>. More recently, it has been  
11 demonstrated that irradiated SPION target the immunosuppressive tumor environment, and re-  
12 activate the immune defense at the tumor site <sup>40</sup>. Even if iron oxide alone shows no effect, a  
13 synergy may occur between gold and iron by combining the effect of strong dose deposition  
14 and ROS catalysis. This was observed before in the case of particles made of gold and  
15 manganese oxide <sup>41</sup>.

16  
17 *H(Fe;Au) associated with irradiation can induce long-term survival of brain tumor-bearing*  
18 *mice: a case study.* A careful investigation of the long-term surviving mouse treated with both  
19 radiotherapy and H(Fe;Au) was particularly interesting. After radiotherapy, the  
20 bioluminescence intensity decreased continuously during 20 days. Then, from day 39, it started  
21 increasing again, first slowly then bursting, leading finally to the death on day 78. One can  
22 reasonably hope that an additional radiotherapy approximately at day 40, that is 20 days after  
23 the end of the first treatment, would have further improved the survival of this individual. This  
24 would have not required a new injection of radiosensitizing materials, since MRI observations  
25 confirmed by histology show that the hybridosomes® were still at the tumor site.

26  
27 *Intratumoral administration after surgery is appropriate for hybridosomes®-based therapy of*  
28 *GBM.* We believe that these results are encouraging in the context of postoperative radiotherapy  
29 combined with chemotherapy, which is the case for standard of care for GBM. Indeed, the blood  
30 brain barrier (BBB) has remained an impassable obstacle for most chemotherapies and  
31 radiosensitizing agents. Therefore, alternative options are convection assisted delivery (CVD)  
32 and local administration of sustained released chemotherapy, embedded in polymer matrixes  
33 such as Gliadel®. Deposition of a radiosensitization agent during surgery is a particularly  
34 advantageous option. Our results show that the nanoparticles constituting the nanocapsule shell

1 are present and visible *in vivo* at the tumor site for at least two months, allowing enough time  
2 for one or even several cycles of radiotherapy. In addition, we demonstrate that an encapsulated  
3 cargo could be delivered from the hybridosomes® specifically to the tumor cells.

4  
5 *MRI vs bioluminescence.* In the clinic, the diagnosis is made by MRI. For preclinical studies,  
6 bioluminescence is much more convenient, provided that a Luciferase-expressing tumor model  
7 is at hand. Importantly, our comparative results show that both techniques are reasonably  
8 correlated. Some discrepancy may arise from the highly scattering nature of the brain tissues,  
9 resulting in intensity loss at the detector for the more profound tumors. In addition, when  
10 present, the SPION hinders the measurements of small tumors. The position of the mouse  
11 relatively to the bioluminescence detector is also an important factor<sup>42</sup>. In addition, in contrast  
12 to bioluminescence, MRI may not account for isolated tumor cells which in the case of GBM,  
13 may extend several centimeters away from the main tumor.

## 14 15 **Conclusion**

16 The current study demonstrates that mixed gold – iron oxide hybridosomes® have a real  
17 potentiating effect on radiotherapy treatment of GBM, with a significant increase of survival  
18 even for a very low amount of gold. Numerous studies (especially simulations and theoretical  
19 calculations) tend to show that the potentiating effect of radiosensitizing nanoparticles is  
20 drastically impacted by their state of aggregation and organization.<sup>43,44</sup> In hybridosomes®, the  
21 assembly of gold nanoparticles into a robust nanocapsule is certainly the key to their  
22 performance in terms of potentiating applied radiation. We are currently investigating this  
23 hypothesis in the laboratory. The decrease of tumoral activity observed for a number of mice  
24 well-responding to this treatment is extremely encouraging, as well as the long-term survival  
25 (78 days) of one individual. Since nanoparticles were still at the tumor site at this time,  
26 additional radiotherapy cycles can be considered for an improved benefit.

27 Moreover, while iron oxide nanoparticles were not effective to enhance the radiotherapy, they  
28 enabled particle tracking and could further be used in the clinics for image-guided radiotherapy.  
29 In addition, cellular and *in vivo* studies have shown that a molecule of interest, concentrated  
30 under its nanoprecipitated form in hybridosomes®, is internalized by the cells and remains  
31 durably in the tumor.

32 Based on these results, we believe that gold-containing hybridosomes® have a great potential  
33 for treatments requiring combined-modality therapy, including surgery, radiotherapy and  
34 chemotherapy, as it is the case for glioblastoma. Few objects present such potentialities.

- 1 Optimization of the gold content and combination with an encapsulated chemotherapy should  
2 further improve the benefits and enable translation of this innovative strategy into the clinics.  
3
- 4 1. Aubry, M. *et al.* From the core to beyond the margin: a genomic picture of glioblastoma  
5 intratumor heterogeneity. *Oncotarget*; Vol 6, No 14 (2015).
  - 6 2. Stupp, R. *et al.* Radiotherapy plus Concomitant and Adjuvant Temozolomide for  
7 Glioblastoma. *N Engl J Med* **352**, 987–996 (2005).
  - 8 3. Wang, Z., Yang, G., Zhang, Y. Y., Yao, Y. & Dong, L. H. A comparison between oral  
9 chemotherapy combined with radiotherapy and radiotherapy for newly diagnosed  
10 glioblastoma: A systematic review and meta-analysis. *Medicine* **96**, e8444 (2017).
  - 11 4. Weller, M., Cloughesy, T., Perry, J. R. & Wick, W. Standards of care for treatment of  
12 recurrent glioblastoma—are we there yet? *Neuro-Oncology* **15**, 4–27 (2013).
  - 13 5. Sarkaria, J. N. *et al.* Is the blood–brain barrier really disrupted in all glioblastomas? A  
14 critical assessment of existing clinical data. *Neuro-Oncology* **20**, 184–191 (2017).
  - 15 6. Clavreul, A., Pourbaghi-Masouleh, M., Roger, E. & Menei, P. Nanocarriers and nonviral  
16 methods for delivering antiangiogenic factors for glioblastoma therapy: the story so far.  
17 *IJN* **14**, 2497–2513 (2019).
  - 18 7. Ashby, L. S., Smith, K. A. & Stea, B. Gliadel wafer implantation combined with standard  
19 radiotherapy and concurrent followed by adjuvant temozolomide for treatment of newly  
20 diagnosed high-grade glioma: a systematic literature review. *World Journal of Surgical*  
21 *Oncology* **14**, 225 (2016).
  - 22 8. Séhédic, D. *et al.* Locoregional Confinement and Major Clinical Benefit of 188Re-  
23 Loaded CXCR4-Targeted Nanocarriers in an Orthotopic Human to Mouse Model of  
24 Glioblastoma. *Theranostics* **7**, 4517–4536 (2017).
  - 25 9. Zhang, H. *et al.* Glioblastoma Treatment Modalities besides Surgery. *J Cancer* **10**, 4793–  
26 4806 (2019).

- 1 10. Fisher, J. P. & Adamson, D. C. Current FDA-Approved Therapies for High-Grade  
2 Malignant Gliomas. *Biomedicines* **9**, 324 (2021).
- 3 11. Butterworth, K. T., McMahon, S. J., Currell, F. J. & Prise, K. M. Physical basis and  
4 biological mechanisms of gold nanoparticle radiosensitization. *Nanoscale* **4**, 4830 (2012).
- 5 12. Coulter, J. A., Hyland, W. B., Nicol, J. & Currell, F. J. Radiosensitising Nanoparticles as  
6 Novel Cancer Therapeutics — Pipe Dream or Realistic Prospect? *Clinical Oncology* **25**,  
7 593–603 (2013).
- 8 13. Rancoule, C. *et al.* Nanoparticles in radiation oncology: From bench-side to bedside.  
9 *Cancer Letters* **375**, 256–262 (2016).
- 10 14. Xie, J. *et al.* Emerging Strategies of Nanomaterial-Mediated Tumor Radiosensitization.  
11 *Advanced Materials* **31**, 1802244 (2019).
- 12 15. Hainfeld, J. F., Dilmanian, F. A., Slatkin, D. N. & Smilowitz, H. M. Radiotherapy  
13 enhancement with gold nanoparticles. *Journal of Pharmacy and Pharmacology* **60**, 977–  
14 985 (2008).
- 15 16. Hainfeld, J. F., Slatkin, D. N. & Smilowitz, H. M. The use of gold nanoparticles to  
16 enhance radiotherapy in mice. *Phys. Med. Biol.* **49**, N309–N315 (2004).
- 17 17. Shariati, M. The Cancer therapy materialization by Theranostic nanoparticles based on  
18 gold doped Iron oxide under electromagnetic field amplification. *Nanomedicine:*  
19 *Nanotechnology, Biology and Medicine* 102406 (2021)  
20 doi:<https://doi.org/10.1016/j.nano.2021.102406>.
- 21 18. Sciortino, F. *et al.* Simple Engineering of Polymer-Nanoparticle Hybrid Nanocapsules.  
22 *ChemNanoMat* **2**, 796–799 (2016).
- 23 19. Gauffre, F., Sciortino, F., Casterou, G., Kahn, M. L. & Chevance, S. Assemblies of  
24 hydrophobic nanoparticles in an aqueous medium, PCT/FR2016/053522. (2017).

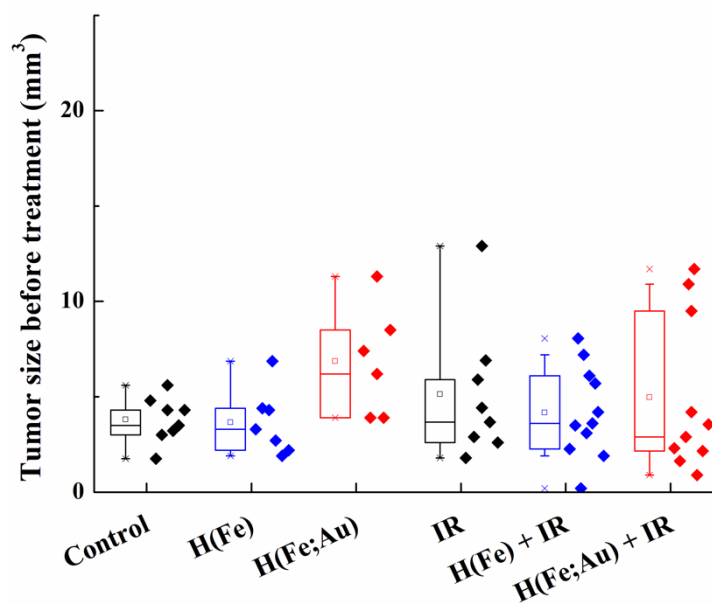
- 1 20. Goubault, C. *et al.* The Ouzo effect: A tool to elaborate high-payload nanocapsules.  
2 *Journal of Controlled Release* (2020) doi:10.1016/j.jconrel.2020.05.023.
- 3 21. Ulrich, G. & Ziessel, R. Convenient and Efficient Synthesis of Functionalized  
4 Oligopyridine Ligands Bearing Accessory Pyrromethene-BF<sub>2</sub> Fluorophores. *J. Org.*  
5 *Chem.* **69**, 2070–2083 (2004).
- 6 22. Casterou, G. *et al.* Improved Transversal Relaxivity for Highly Crystalline Nanoparticles  
7 of Pure  $\gamma$ -Fe<sub>2</sub>O<sub>3</sub> Phase. *Chem. Eur. J.* **21**, 18855–18861 (2015).
- 8 23. Liu, S., Chen, G., Prasad, P. N. & Swihart, M. T. Synthesis of Monodisperse Au, Ag, and  
9 Au–Ag Alloy Nanoparticles with Tunable Size and Surface Plasmon Resonance  
10 Frequency. *Chem. Mater.* **23**, 4098–4101 (2011).
- 11 24. Clark, A. J. *et al.* Stable luciferase expression does not alter immunologic or in vivo  
12 growth properties of GL261 murine glioma cells. *J Transl Med* **12**, 345 (2014).
- 13 25. Schneider, C. A., Rasband, W. S. & Eliceiri, K. W. NIH Image to ImageJ: 25 years of  
14 image analysis. *Nature Methods* **9**, 671–675 (2012).
- 15 26. Hennig, J., Friedburg, H. & Ströbel, B. Rapid nontomographic approach to MR  
16 myelography without contrast agents. *J Comput Assist Tomogr* **10**, 375–378 (1986).
- 17 27. Sciortino, F. *et al.* Structure and elasticity of composite nanoparticle/polymer nanoshells  
18 (hybridosomes®). *Soft Matter* **13**, 4393–4400 (2017).
- 19 28. Maes, W. & Van Gool, S. W. Experimental immunotherapy for malignant glioma: lessons  
20 from two decades of research in the GL261 model. *Cancer Immunol Immunother* **60**,  
21 153–160 (2011).
- 22 29. Ferrer-Font, L. *et al.* Metronomic treatment in immunocompetent preclinical GL261  
23 glioblastoma: effects of cyclophosphamide and temozolomide. *NMR in Biomedicine* **30**,  
24 e3748 (2017).

- 1 30. Trofymchuk, K. *et al.* BODIPY-loaded polymer nanoparticles: chemical structure of  
2 cargo defines leakage from nanocarrier in living cells. *J. Mater. Chem. B* **7**, 5199–5210  
3 (2019).
- 4 31. Cho, S. H. Estimation of tumour dose enhancement due to gold nanoparticles during  
5 typical radiation treatments: a preliminary Monte Carlo study. *Phys. Med. Biol.* **50**, N163–  
6 N173 (2005).
- 7 32. Roeske, J. C., Nuñez, L., Hoggarth, M., Labay, E. & Weichselbaum, R. R.  
8 Characterization of the Theoretical Radiation Dose Enhancement from Nanoparticles.  
9 *Technol Cancer Res Treat* **6**, 395–401 (2007).
- 10 33. Wilhelm, S. *et al.* Analysis of nanoparticle delivery to tumours. *Nat Rev Mater* **1**, 16014  
11 (2016).
- 12 34. Bhattarai, S. R. *et al.* Gold nanotriangles: scale up and X-ray radiosensitization effects in  
13 mice. *Nanoscale* **9**, 5085–5093 (2017).
- 14 35. Liu, S. *et al.* Radiosensitizing effects of different size bovine serum albumin-templated  
15 gold nanoparticles on H22 hepatoma-bearing mice. *Nanomedicine* **13**, 1371–1383 (2018).
- 16 36. Luo, D. *et al.* Prostate-specific membrane antigen targeted gold nanoparticles for prostate  
17 cancer radiotherapy: does size matter for targeted particles? *Chem. Sci.* **10**, 8119–8128  
18 (2019).
- 19 37. Mowat, P. *et al.* In Vitro Radiosensitizing Effects of Ultrasmall Gadolinium Based  
20 Particles on Tumour Cells. *J. Nanosci. Nanotech.* **11**, 7833–7839 (2011).
- 21 38. Kirakli, E. K. *et al.* Superparamagnetic iron oxide nanoparticle (SPION) mediated in vitro  
22 radiosensitization at megavoltage radiation energies. *Journal of Radioanalytical and*  
23 *Nuclear Chemistry* **315**, 595–602 (2018).

- 1 39. Rashid, R. A. *et al.* Radiosensitization effects and ROS generation by high Z metallic  
2 nanoparticles on human colon carcinoma cell (HCT116) irradiated under 150 MeV proton  
3 beam. *OpenNano* **4**, 100027 (2019).
- 4 40. Wu, C. *et al.* Repolarization of myeloid derived suppressor cells via magnetic  
5 nanoparticles to promote radiotherapy for glioma treatment. *Nanomedicine:*  
6 *Nanotechnology, Biology and Medicine* **16**, 126–137 (2019).
- 7 41. Chen, G., Roy, I., Yang, C. & Prasad, P. N. Nanochemistry and Nanomedicine for  
8 Nanoparticle-based Diagnostics and Therapy. *Chem. Rev.* **116**, 2826–2885 (2016).
- 9 42. Keyaerts, M., Caveliers, V. & Lahoutte, T. 4.16 - Bioluminescence Imaging. in  
10 *Comprehensive Biomedical Physics* (ed. Brahme, A.) 245–256 (Elsevier, 2014).  
11 doi:10.1016/B978-0-444-53632-7.00418-4.
- 12 43. Retif, P. *et al.* Nanoparticles for Radiation Therapy Enhancement: the Key Parameters.  
13 *Theranostics* **5**, 1030–1044 (2015).
- 14 44. Retif, P. *et al.* Monte Carlo simulations guided by imaging to predict the in vitro ranking  
15 of radiosensitizing nanoparticles. *IJN Volume* **11**, 6169–6179 (2016).  
16

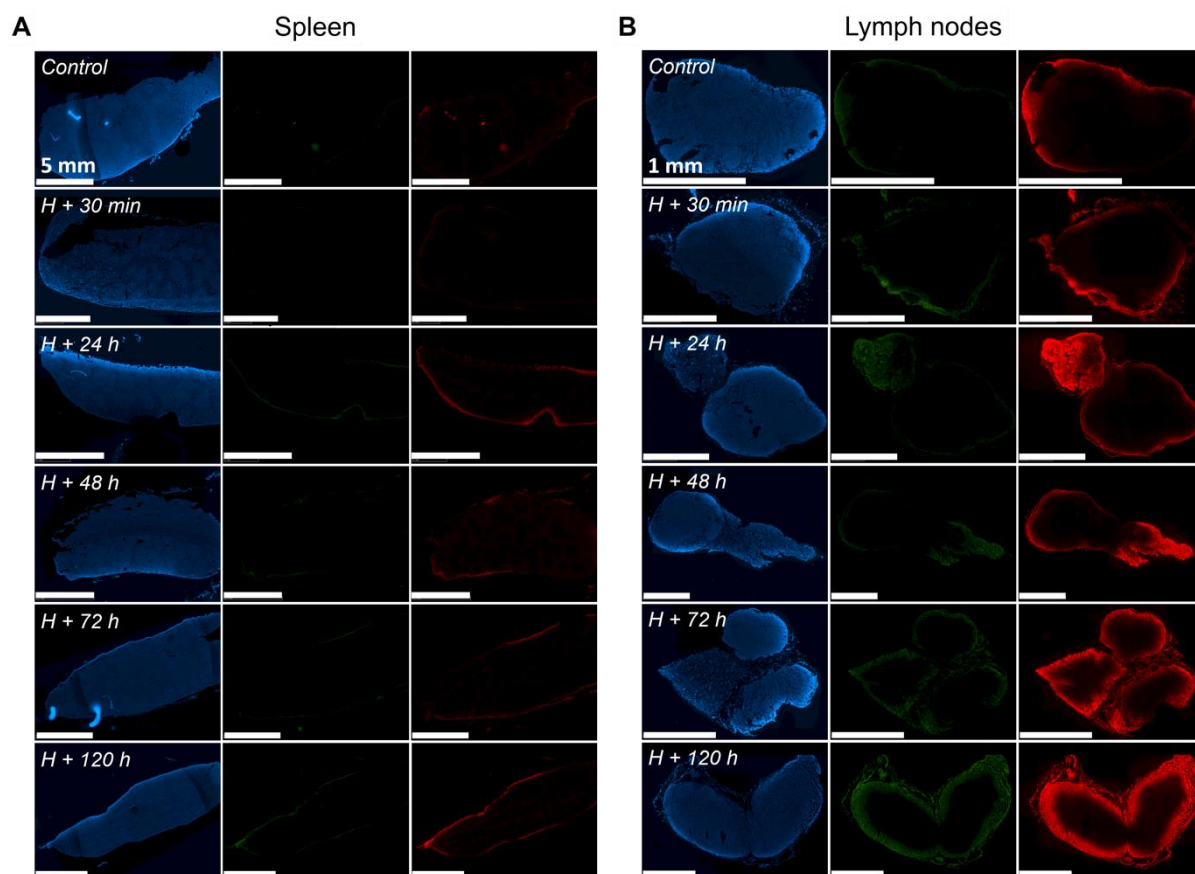
1  
2  
3

## Supplemental Figures

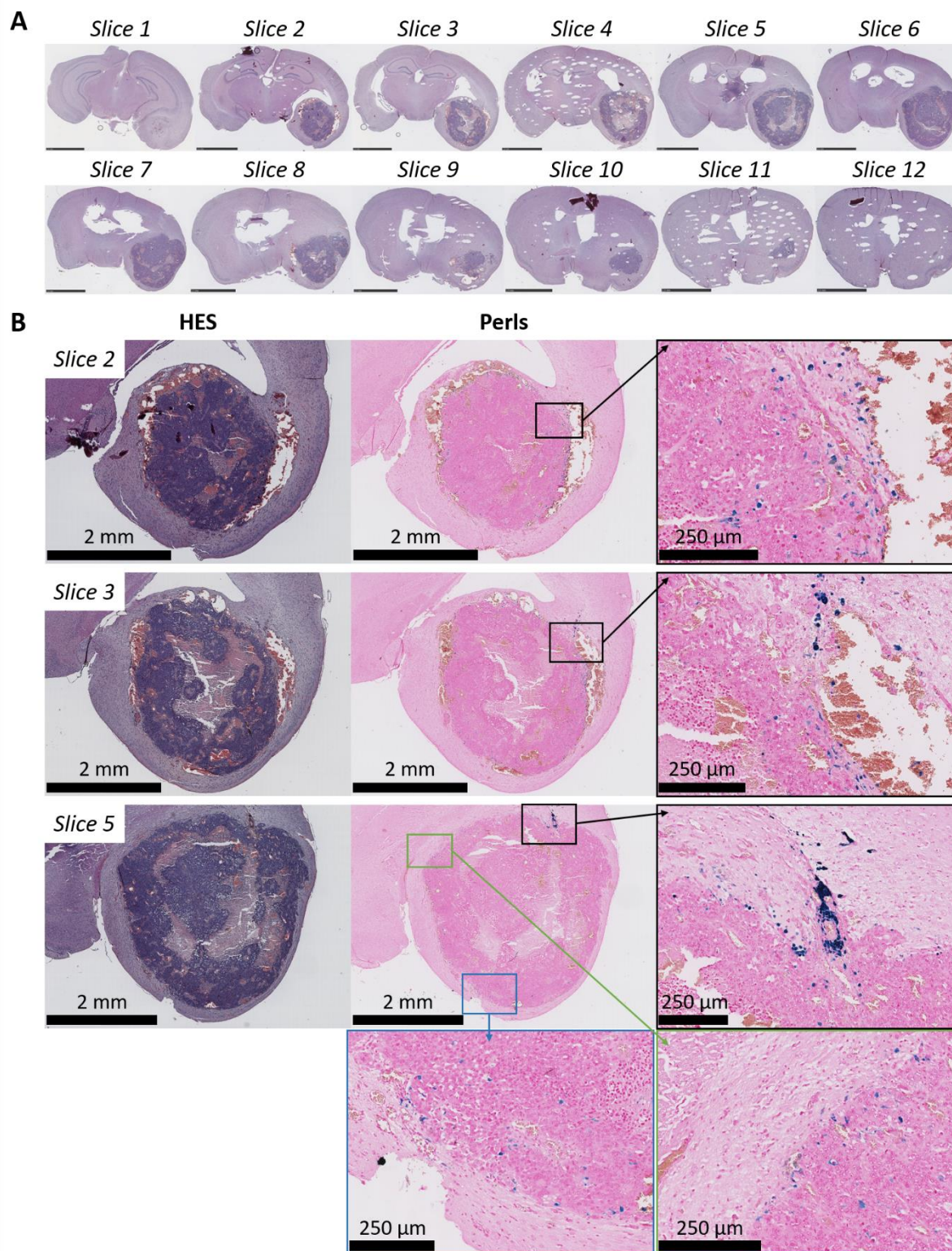


4  
5  
6  
7  
8

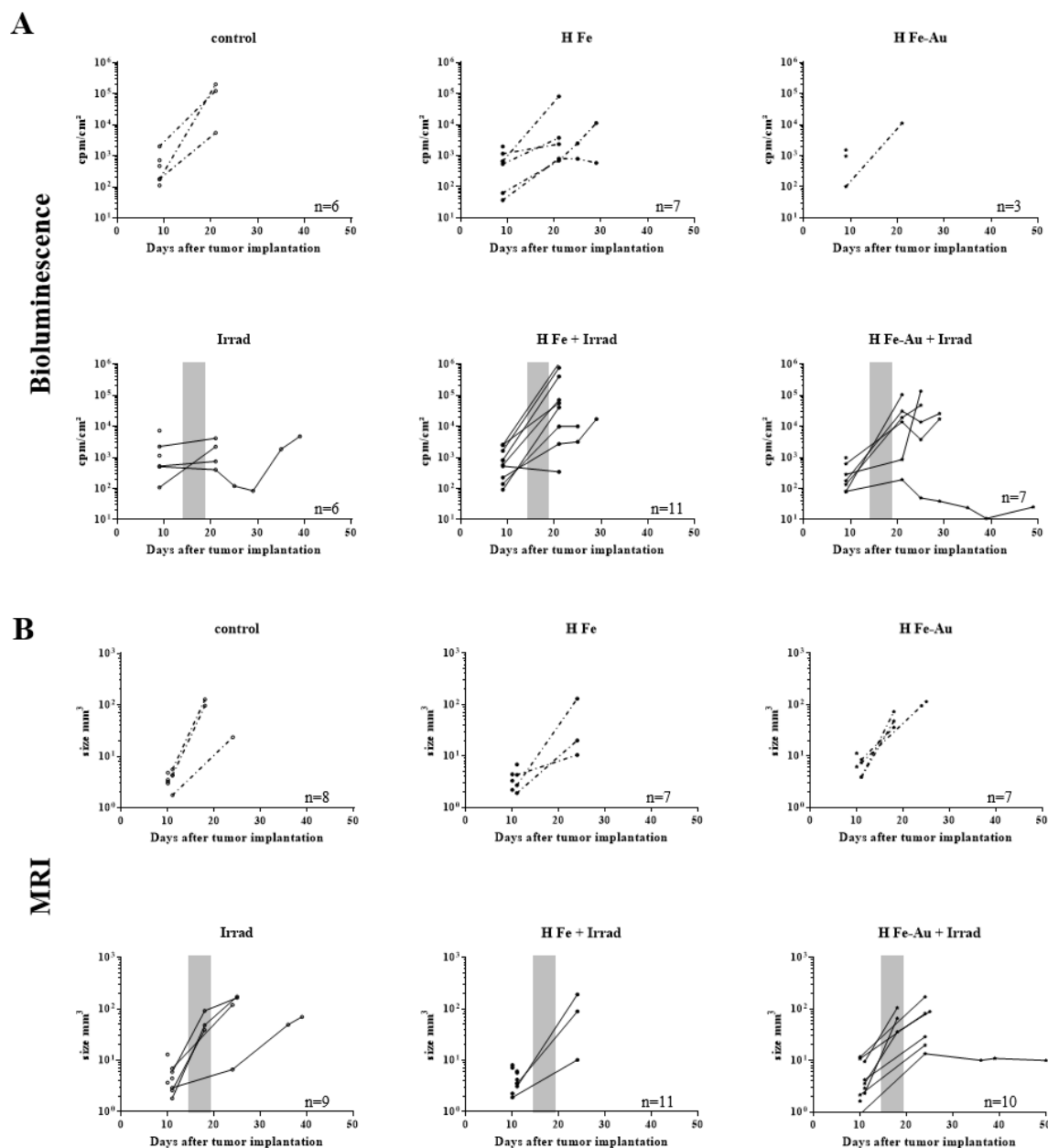
**Figure SI-1** – Initial tumor size distribution (day 9/10) within the 6 groups of mice. The inner walls in the boxes represent the median. The lower and upper walls of the boxes represent respectively the 1<sup>st</sup> and 3<sup>rd</sup> quartiles. Lower and upper ticks represent the 1<sup>st</sup> and 9<sup>th</sup> deciles.



1  
2 **Figure SI- 2** – Confocal microscopy fluorescence of slices of (A) spleen and (B) cervical lymph nodes of mice at  
3 different times after intratumoral injection (t=0) of BODIPY-loaded H(Fe). Tissues were stained with DAPI and  
4 imaged for DAPI (blue) and BODIPY (green+red) fluorescence.



1  
2 **Figure SI-3** – Microscopy observations of slices of the brain of mouse #1082, after HES and Perls  
3 staining. (A) Slices (1 to 12) were performed every 100  $\mu$ m. (B) Enlargement centered on the tumor, of  
4 slices 2; 3 and 5, with HES and Perls staining. Iron (blue) is clearly present at the edges of the tumor.  
5  
6



1  
2 **Figure SI- 4** Bioluminescence and MRI follow-up. The hybridosomes® H(Fe) or H(Fe;Au) were  
3 intratumorally injected at day 14 or 16 after GL261-Luc+ cells brain implantation. Irradiation started at  
4 the time of injection, for 5 days. Mice were monitored by (A) Bioluminescence (intensity) and (B) MRI  
5 (tumor volume). The grey zone represents the radiotherapy sessions.

6  
7  
8

